WCTE 2021
WORLD CONFERENCE ON TIMBER ENGINEERING
SANTIAGO, CHILE | 9 - 12 AUGUST

PINCHING EFFECT ON SEISMIC PERFORMANCE OF A SDOF LIGHT-FRAME TIMBER STRUCTURE

Ariya Eini[1], Lina Zhou[1], Chun Ni[2]

ABSTRACT: Although energy dissipation is one of the key factors in resisting seismic force, current design codes only take into account the ductility of the backbone properties of hysteresis curves, and the energy dissipation is usually not accounted for. This paper focuses on understanding and assessing the influence of energy dissipation due to different pinching levels on the seismic performance of a light-frame wood shear wall system. Timber structures with identical backbone curves but different pinching levels were analyzed. Incremental dynamic analyses were run on a single-degree-of-freedom system with varying pinching stiffness and residual strength. The seismic evaluation is presented by the spectral accelerations causing failure of the structure and the hysteresis energy dissipation under a suite of 22 ground motions (2 components per motion) over a wide range of fundamental periods of typical timber structures. Results show that the effect of pinching on the seismic performance of timber structures is period-dependent. Short period structures are more sensitive to the pinching of hysteresis loops compared to long period structures. The residual strength of pinching loops has a greater influence on the seismic performance than the stiffness of the pinching loops. Hysteretic energy dissipation derived from standard reversed-cyclic tests can provide a better understanding on the seismic resistance of timber structures. However, the hysteretic energy under a seismic event at near-collapse stage neither agrees with quasi-static cyclic test's energy dissipation nor is well correlated to the maximum seismic capacity of the structure.

KEYWORDS: Light-frame wood structure, Pinching effect, IDA analysis, SDOF system, Seismic performance, Hysteretic energy dissipation

1 INTRODUCTION

Most common seismic design practices rely on the ductility and damping of the structural system to dissipate energy under seismic load. The ductility factor is defined as the ratio of the deformation at the failure stage to the deformation at yield. So, it is derived from the backbone of the hysteresis curves without including the effect of pinching on the energy dissipation of the structure. In timber construction, notably light-frame shear wall systems, the force-deformation relationship is usually highly nonlinear and pinched. The current seismic design codes only account for the characteristics of backbone curves, i.e., two systems with an identical backbone have the same seismic design parameters.

However, previous studies have shown that the strength and stiffness degradation, and pinching of hysteresis loops do affect the seismic response of structures. Hyung Lee et al. [1] established the functional form of ductility response modification factor (R_μ) based on various hysteretic models, including pinched hysteresis with different residual strength. A lower R_μ was obtained with an increase of pinching level. A study by Paevere and Foliente [2] focused on generating response statistics for generic single-degree-of-freedom (SDOF) oscillators from a tri-linear model to full degrading and pinching models. The pinching branch of hysteresis was assumed to have zero residual strength and stiffness with a pinching width of zero. The results demonstrated up to a 100% variation in maximum displacement and energy dissipation values throughout the models. They also showed a 50% variation in reliability index. Medina and Krawinkler [3] evaluated the sensitivity of roof and maximum story drifts of frame structures to three hysteresis types: peak-oriented, bilinear and pinching. They found that displacement demands are higher in pinching model and more evident in multi-degree-of-freedom (MDOF) systems than SDOF. Another study on probabilistic characteristics of inelastic SDOF systems revealed that degradation parameters of hysteresis loop had significant effect on ductility demand; and the pinching effects amplified seismic response [4]. Pu and Wu [5] Compared bilinear hysteretic SDOF systems with pinched hysteresis and concluded that pinching hysteretic structures are more affected by seismic sequences. They also had higher ductility amplification ratios.

Hysteretic yielding energy (Ey) has proven to be a key factor in seismic capacity of structures and researchers have been trying to establish damage indexes to correlate Ey and hysteresis properties. A study on the distribution of Ey and input energy of MDOF systems with different hysteresis loops showed that Ey demand varies in the

[1] Ariya Eini, Department of Civil Engineering, University of Victoria, Canada, ariyaeini@uvic.ca
Lina Zhou, Department of Civil Engineering, University of Victoria, Canada, linazhou@uvic.ca

[2] Chun Ni, FPInnovations, Canada, chun.ni@fpinnovations.ca

following order: Bilinear Plastic > Strength Degradation > Bilinear Flag > Bilinear Slip [6]. Molazadeh et.al [7] demonstrated that in short-period models with effects of pinching-degrading (among models with different degrees of stiffness and strength degradation), the ground motion duration influences the central tendency of Ey and ductility demand significantly. Kazantzi and Vamvatsikos [8] conducted incremental dynamic analysis (IDA) on kinematic hardening model, curved kinematic hardening model, peak-oriented model, flag-shaped model, pinching model, and nonlinear elastic model. No consistent correlation was found between Ey dissipation and seismic performance (acceleration and displacement demand).

The above-mentioned studies explored the seismic performance of elasto-plastic non-degrading structures in comparison to systems with cyclic and in-cycle strength and stiffness degradation or pinching effects. And most of them are derived from hysteresis loops for typical steel and reinforced concrete structures. It is not clear how hysteresis parameters associated with varying severity of pinching phenomenon affects the seismic performance of timber structures. Herein, numerical models of a light-frame shear wall system with different pinching levels and fundamental periods were developed via OpenSees [9] to investigate the performance of timber structures under a suite of 22 ground motions.

2 NUMERICAL MODELING ANALYSIS

2.1 HYSTERETIC MODEL

SAWS model [10] in OpenSees [9] was adopted in this project to simulate the hysteresis performance of wood shear walls. The force-deformation paths in SAWS model have a segmental linear relationship, except the path following the envelope curve until the peak load (load relative to DU in Figure 1). The unloading path includes two segments, the elastic unloading phase and the pinched unloading phase. . Unloading continues on this path until the loading in the opposite direction happens. The slope of this branch (pinching stiffness), along with zero-displacement intercept (residual strength), represents the level of pinching.

There are ten parameters in the SAWS model (Figure1) to describe the hysteresis loops, in which S0 is the initial stiffness of the structure; R4 is the ratio of the pinching stiffness to the initial stiffness, and FI is the residual strength of the system, etc. To obtain the SAWS hysteresis characteristics, a simple shear wall model was developed in OpenSees with three rigid elements and one bracing diagonal spring shown in Figure 2. It is a 2D simulation of the shear wall with pin support connections. A fitting procedure was employed to calibrate these 10 parameters based on a quasi-static reversed cyclic test of a wood shear wall by Zhou [11]. Figure 3 shows the comparison of the numerical hysteresis loops of the reference case (model S1 in Table 1) with experimental hysteresis loops. Figure 4 is a presentation of the cyclic cumulative energy of the calibrated numerical model (S1) which is in good agreement with the test data by a difference of ±5%. The 10 calibrated parameters for S1 are listed in Table 1.

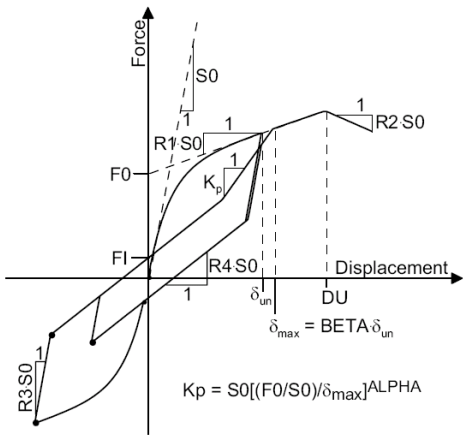

Figure 1: *SAWS-10 parameters model [10]*

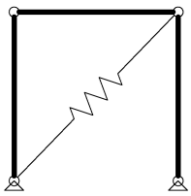

Figure 2: *Schematic of the 2D shear wall model.*

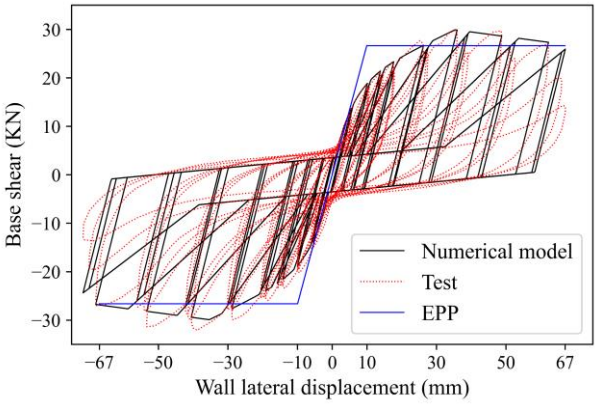

Figure 3: *Comparison of hysteresis loops of the test and the numerical model (S1)*

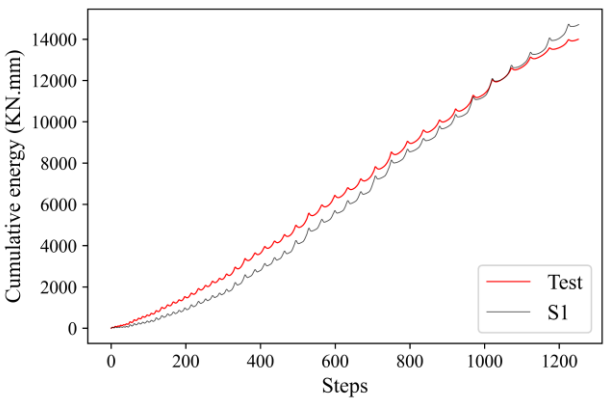

Figure 4: *Comparison of hysteretic energy between the test data and the numerical model (S1)*

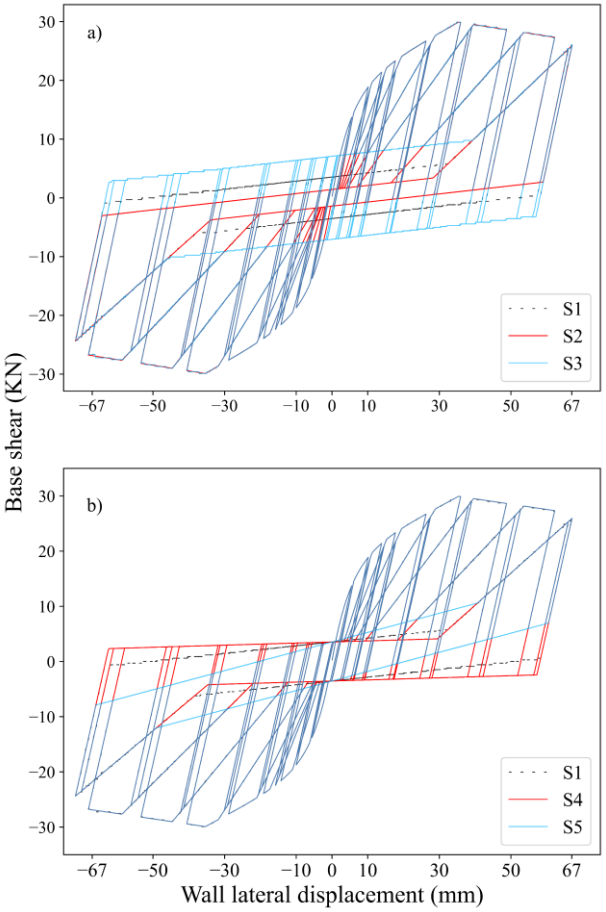

Figure 5: *Comparison of reference case (S_1) hysteresis loop with models of different a) residual strength (S_2 and S_3), and b) different pinching stiffness (S_4 and S_5).*

2.2 STRUCTURES WITH VARYING PINCHING LEVEL

Having a pinching hysteresis is a major feature of light-frame timber structures. Their hysteretic shape is more pinched in the middle compared to steel and concrete structures. As the magnitude of the cyclic loading increases, fasteners crush the wood fibers, causing

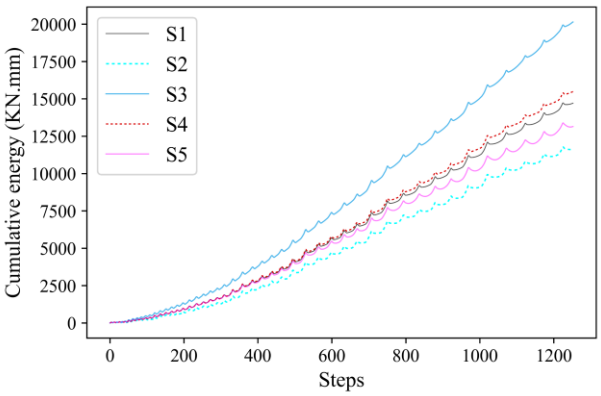

Figure 6: *Comparison of hysteretic energy between the reference case (S1) and other developed models.*

permanent gaps between the fastener and wood material. When the nails loaded in the opposite direction passing through the gaps, they face a reduced resistance due to indented wood [12]. Softening of the fasteners and crushing of wood fibers make the area under the force-deformation curves pinched. The main characteristics of hysteresis loops attributed to the pinching effect is where a stiffness degradation happens in the unloading and reloading in the opposite direction of the system. As a result, the system cannot reach the same strength until reloading in the reversed direction when the fasteners fully touch the wood material again. Therefore, the pinching degree is controlled by both the intercept strength of the pinching branch (residual strength) and its stiffness.

With the aim of assessing the pinching effect, it has to be isolated from all other features of the hysteresis loop. In addition to S1, which is the model validated by test results, four other pinching models with the same backbone curve and different residual strength or pinching stiffness were developed. To assign a realistic range of values for pinching stiffness and residual strength, a group of former test results was taken into consideration [13-23]. The ratio of the pinching stiffness to the elastic stiffness and ratio of residual strength to yield strengths accounts for the severity of pinching

Table1*: Hysteretic Parameters for Shear Wall spring elements*

Models	S0(KN)	DU	α	ß	R1	R2	R3	R4	F0 (KN)	FI (KN)
S_1(reference)	7.7	25	0.7	1.1	0.09	-0.025	0.75	0.018	25	5
S_2	7.7	25	0.7	1.1	0.09	-0.025	0.75	0.018	25	2
S_3	7.7	25	0.7	1.1	0.09	-0.025	0.75	0.018	25	10
S_4	7.7	25	0.7	1.1	0.09	-0.025	0.75	0.005	25	5
S_5	7.7	25	0.7	1.1	0.09	-0.025	0.75	0.045	25	5

Table2*: Comparison of all models' quasi-static cyclic cumulative hysteretic energy.*

Models	S1	S2	S3	S4	S5	EPP
Energy (KN.mm)	14707	11621	20144	15478	13147	51600
(Energy / S1 Energy) ratio	1.00	0.79	1.37	1.05	0.89	3.51

effect. It was observed from cyclic tests that these two stiffness and strength ratios typically change between 0.05% to 0.45% and 5% to 27%, respectively. Therefore, two other models named S2 and S3 shown in Figure 5a with the same hysteretic characteristics of S1 but difference residual strength, FI, were developed. To consider the pinching stiffness variable, the lower and upper bound of R4 was assigned to two more models (S4 and S5 in Figure 5b). Table 1 lists the 10 parameters for all SAWS models. An Elastic Perfectly Plastic (EPP) model based on the equivalent energy elastic-plastic method [24] derived from the backbone of test hysteresis loops was also investigated (Figure 3).

The Cumulative energy from quasi-static test loading for five SAWS models and the EPP model is demonstrated in Table 2. Figure 6 presents the energy dissipation history of the all developed models. With the exception of EPP, it is obvious that S2 with respect to S1 has the lowest and S3 has the highest energy dissipation capacity based on the cyclic test loading. S4 and S5 have higher and lower energy dissipation, respectively, compared to S1. That means an increase in residual strength of pinching branch adds to the quasi-statically absorbed energy. Conversely, the pinching stiffness has an inverse correlation in that respect. Also, altering the residual strength to its extreme expected values leads to a greater effect on the quasi-statically hysteresis energy than changing the pinching stiffness to its extremes.

2.3 INCREMENTAL DYNAMIC ANALYSIS

To investigate a complete range of seismic response versus the range of possible levels of a ground motion record, the incremental dynamic analysis (IDA) [25] is adopted. As the IDA results are highly dependent on the record-to-record variability, a suite of 22 far-field ground motions (two components per motion) from FEMA P-695 [26] were selected. The intensity measure (IM) was represented by spectral acceleration (Sa) at the fundamental period of the SDOFs, and the damage measure (DM) was chosen to be the displacement at the top of the wall. The energy of the earthquake imparted to the system needs to be dissipated through damping and hysteresis mechanisms. The input energy also depends on the period of the structure. In this research, twelve fundamental periods (0.1s, 0.2s, 0.3s, 0.4s, 0.5s, 0.6s, 0.7s, 0.8s, 0.9s, 1s, 1.5s, 2s) that cover the common periods of timber structures in practice were analyzed for each hysteretic model by changing the assigned mass and keeping the same stiffness (K_{EPP}) of the models. Mass was lumped at the top two nodes of the wall (Figure 2). The viscous damping ratio of 1% was applied as suggested in [27]. Although some references reported higher critical damping but the purpose of this study was to show the significance of yielding hysteresis energy, so the lower bound was selected.

IDA was carried out on the 72 SDOF systems by scaling up each record to reach the failure stage, which happens at 67 mm lateral deformation based on test backbone curve (Figure 3). Both components of seismic events were used for the 22 ground motions, and a total of 63360 nonlinear dynamic analyses were run. The secondary collapse criterion was based on the IDA curves (spectral acceleration vs. maximum lateral displacement) when the tangent slope of the IDA curve equals 20% of the initial slope [28].

Since a high-capacity resolution of IDA curves was needed in this study, a high concentration of IM values around the failure limit was primarily chosen to better bracket the flatline at near-collapse stage. Having closed the distance between the highest non-collapsing IM and the lowest collapsing IM, the exact point in which the DM values fall within a tolerance of 1 mm of the primary failure criterion was found. Once the failure capacity of the system on each single-record curve was obtained, other grid points were evenly spread to twenty steps. Filling the gaps at lower IMs creates non-matching levels that leads to the need for interpolation. The cross-sectional median method was used to summarize the IDA curves. The median curves flatten when collapse occurs in 50% of records. Figure 7 shows the density of each 44 single-record IDA grid point of S1 model with a vibration period of 0.3 sec. The same procedure was followed for the cumulative hysteretic energy dissipation analysis. It is calculated by the sum of the area under hysteresis loops at each intensity level. Yielding hysteretic energy (Ey) was employed without normalization because the purpose of this study was to assess the energy dissipation capabilities in collapse point and also all models had the same yield strength.

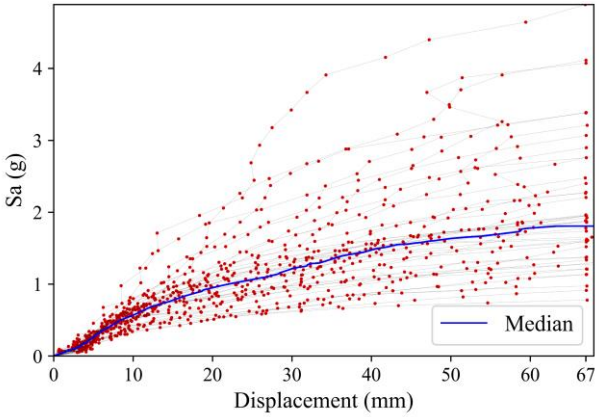

Figure 7: *IDA curves of S1 with period of 0.3s.*

3 RESULTS

Figures 8 presents the median IDA curves for six models with periods of 0.2 sec, 0.7 sec and 2 sec, respectively. These specific results are just illustrated as an example of short and long period structures. In these systems, at the early stages of IDA, all models showed similar seismic behavior. When spectral accelerations are large enough, the EPP curve starts to deviate significantly from other pinched models for structures with period of 0.2 sec, but almost shows no difference for 0.7 sec and 2 sec structures.

Generally, for longer period structures (2.0 sec), the IDS curves (Sa versus displacement) are almost linear, which means these plastic systems have similar ultimate displacement compared to their corresponding elastic systems, while for short period structure (0.2s), the slope of the curves decreases when displacement increases

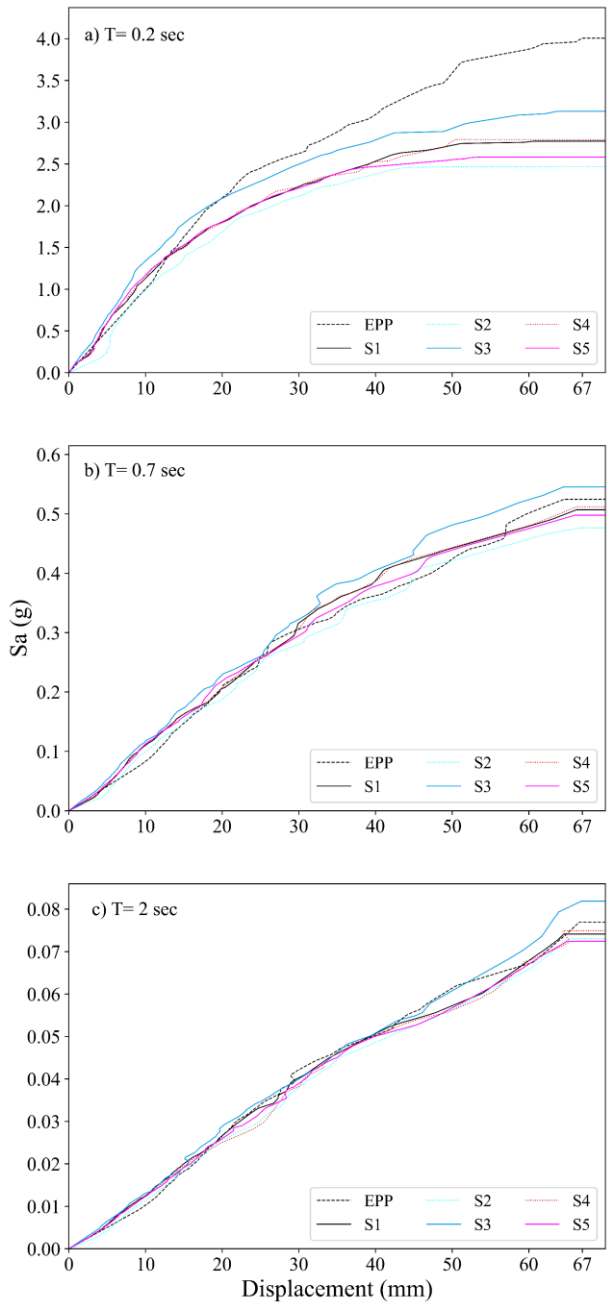

Figure 8: *Median IDA curves (Sa vs Displacement) for models with with a) T = 0.2 sec, b) T = 0.7 sec, and c) T = 2 sec*

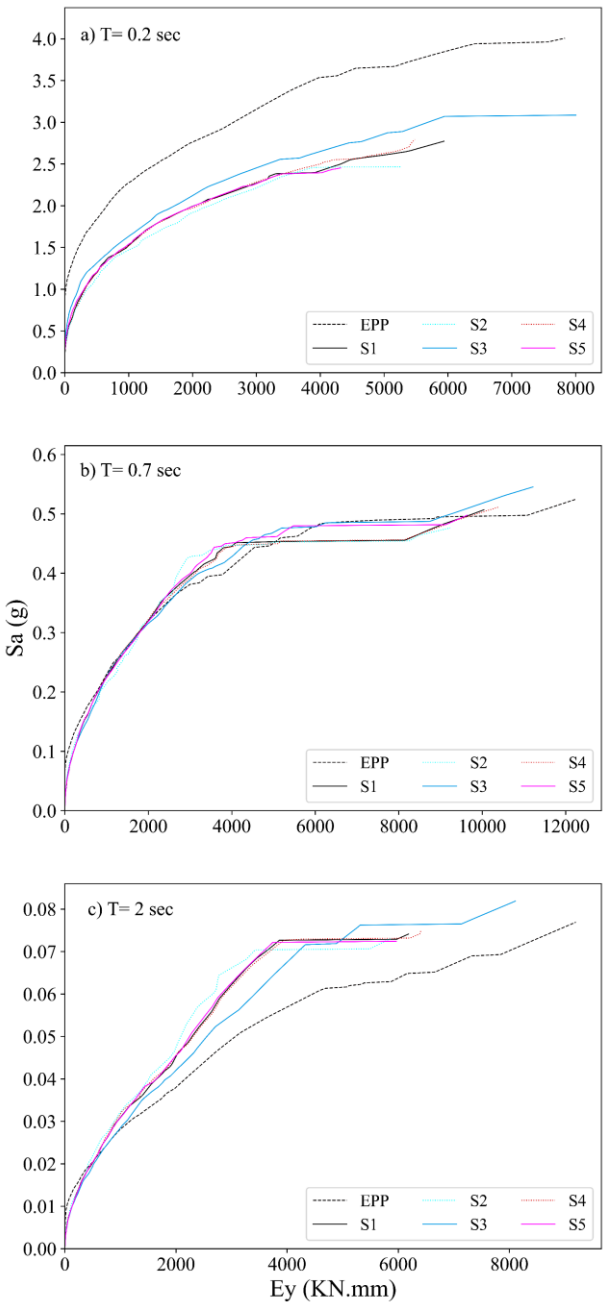

Figure 9: *Median IDA curves (Sa vs Ey) for models with a) T = 0.2 sec, b) T = 0.7 sec, and c) T = 2 sec*

(Figure 8a), which indicates the ultimate displacement of these systems is larger than their corresponding elastic systems. Among pinching models, S3 with largest residual strength has the highest collapse capacity and S2 with smallest residual strength has the lowest capacity. The difference among S4, S5 and S1 is much smaller than that among S3, S2 and S1. Generally, S4 with smaller pinching stiffness has relatively larger ultimate capacity. This distinction was more pronounced at periods lower than 0.7s. Although, S3 always showed a higher seismic capacity than S1 throughout the entire spectrum. For long period structures such as the ones with period of 2s (Figure 8c) only marginal differences between models' response exist. The IDA curves based on cumulative yielding energy (Ey) are presented in Figure 9.

EPP with a period of 0.2s has less EY than other pinching models at the same ground motion intensity level. S5 has the lowest and S3 has the highest Ey at collapse. The Ey values (Figure 9a) are not in the same order as the seismic capacity (Figure 8a) at period of 0.2s. Models with period of 0.7s showed similar values of Ey at different performance levels. Figure 9c demonstrates that EPP with period of 2s has higher energy dissipation at the same IM than other pinching models with the same period, and it also has higher Ey at the collapse point.

Normalized spectral accelerations of models at near-collapse stage based on values of S1 is presented in Figure 10 for all periods. It is obvious that specially in periods lower than 0.7 EPP has higher failure capacity. Among pinching models, S3 has the maximum capacity and S2

***Table3**: Median spectral acceleration (Sa(g)) at failure stage and its ratio to Sa of S1*

Period (s) / Models	EPP	S1	S2	S3	S4	S5
0.1	8.814(1.68)*	5.260(1.00)	5.075(0.96)	5.719(1.09)	4.856(0.92)	4.769(0.91)
0.2	4.007(1.44)	2.773(1.00)	2.466(0.89)	3.085(1.11)	2.793(1.01)	2.583(0.93)
0.3	2.330(1.29)	1.806(1.00)	1.687(0.93)	2.039(1.13)	1.803(1.00)	1.800(1.00)
0.4	1.476(1.16)	1.273(1.00)	1.169(0.92)	1.299(1.02)	1.276(1.00)	1.247(0.98)
0.5	1.066(1.10)	0.969(1.00)	0.914(0.94)	1.028(1.06)	1.003(1.04)	0.950(0.98)
0.6	0.804(1.18)	0.680(1.00)	0.635(0.93)	0.745(1.10)	0.691(1.02)	0.667(0.98)
0.7	0.525(1.03)	0.507(1.00)	0.476(0.94)	0.545(1.08)	0.512(1.01)	0.498(0.98)
0.8	0.403(0.95)	0.426(1.00)	0.365(0.86)	0.445(1.05)	0.426(1.00)	0.403(0.95)
0.9	0.341(0.89)	0.382(1.00)	0.346(0.90)	0.394(1.03)	0.381(1.00)	0.348(0.91)
1	0.281(1.09)	0.258(1.00)	0.246(0.95)	0.283(1.10)	0.261(1.01)	0.258(1.00)
1.5	0.148(1.14)	0.130(1.00)	0.132(1.02)	0.155(1.20)	0.134(1.03)	0.137(1.06)
2	0.077(1.04)	0.074(1.00)	0.073(0.99)	0.082(1.10)	0.075(1.01)	0.072(0.98)

*Spectral acceleration ratio of each model to the S1 model with the same period.

***Table4**: Median hysteretic energy (Ey) at failure stage (KN.mm) and its ratio to Ey of S1*

Period (s) / Models	EPP	S1	S2	S3	S4	S5
0.1	4455(0.70)*	6332(1.00)	5290(0.84)	8133(1.28)	4465(0.71)	3374(0.53)
0.2	7833(1.32)	5940(1.00)	5276(0.89)	8003(1.35)	5482(0.92)	4317(0.73)
0.3	14708(1.12)	13122(1.00)	9417(0.72)	14533(1.11)	13037(0.99)	12896(0.98)
0.4	9385(1.33)	7042(1.00)	6052(0.86)	7621(1.08)	7086(1.01)	7309(1.04)
0.5	11118(1.04)	10686(1.00)	10539(0.99)	11998(1.12)	12319(1.15)	10747(1.01)
0.6	13394(1.62)	8261(1.00)	7564(0.92)	12210(1.48)	8401(1.02)	9650(1.17)
0.7	12241(1.22)	10040(1.00)	9233(0.92)	11214(1.12)	10407(1.04)	9637(0.96)
0.8	11057(1.17)	9420(1.00)	7081(0.75)	10951(1.16)	9314(0.99)	8856(0.94)
0.9	13401(1.23)	10866(1.00)	6000(0.55)	8925(0.82)	10654(0.98)	7347(0.68)
1	13989(2.13)	6573(1.00)	5534(0.84)	9002(1.37)	6781(1.03)	6515(0.99)
1.5	11034(1.91)	5787(1.00)	5374(0.93)	7965(1.38)	5751(0.99)	6089(1.05)
2	9196(1.49)	6184(1.00)	5857(0.95)	8107(1.31)	6406(1.04)	5963(0.96)

*Hysteretic energy dissipation ratio of each model to the S1 model with the same period.

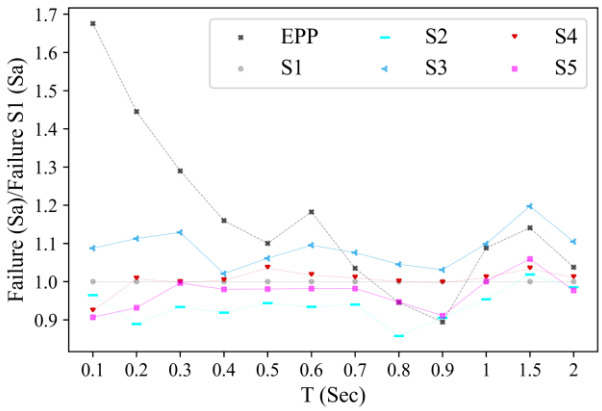

***Figure 10**: Failure median Sa ratio of all models over S1*

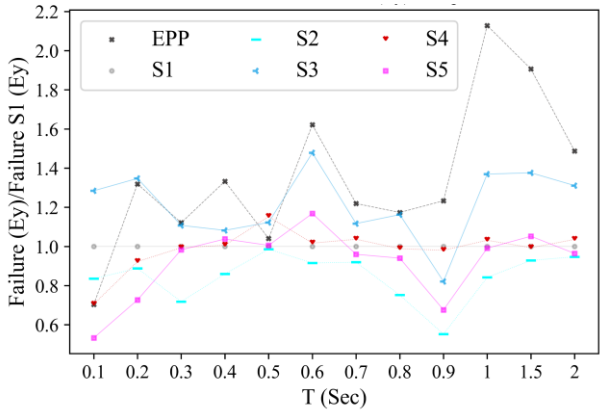

***Figure 11**: Failure median Ey ratio of all models over S1*

has the minimum capacity. S4 has higher capacity compared to S1, except at T = 0.1 sec. S5 shows lower capacity in comparison to S1.

The same presentation for Ey at failure in Figure 11 shows that S2 has significantly less Ey than others in eight period values, and S3 has more Ey in ten period values than

others. But still, no clear interpretation can be made based on Ey values at maximum seismic capacity.

4 CONCLUSION

The purpose of this study was to use IDA to find seismic collapse capacity and hysteresis energy of SDOF light-frame wood shear wall systems with different levels of pinching, which is mainly represented by the parameters of pinching stiffness and residual strength.
The main study findings are summarized as follows:

- higher residual strength of pinching branch leads to higher seismic resistance for short period systems, change of pinching stiffness has less impact on the seismic performance of timber structures.
- A continuation of elastic regime slope until the near-collapse state in IDA curves for long period structures is observed, while short period structures experience softening at a lower level.
- It can be seen that the short period structures are more sensitive to the pinching effect of hysteresis loops than long period structures.
- The Elastic Perfectly Plastic model as a representation of a system with fuller hysteresis has much higher capacity than pinching models, but with periods of more than 0.7s, the difference decreases.
- The hysteresis shape affects the seismic performance but it would more appropriately correlate with hysteretic characteristics (pinching stiffness and residual strength) than solely the hysteretic energy. Even though increasing of quasi-statically hysteretic energy of systems with different pinching degrees could establish the order of seismic capacity but the same conclusion can not be drawn in respect to the Elastic Perfectly Plastic model.
- Care should be exercised when relating seismic capacity to hysteretic energy since not a straightforward relationship exists.

ACKNOWLEDGEMENT

This study is funded by Forestry Innovation Investment Ltd. in BC – Wood First Program.

REFERENCES

[1] Lee, L.H., S.W. Han, and Y.H. Oh: Determination of ductility factor considering different hysteretic models, in Earthquake Engineering & Structural Dynamics. John Wiley & Sons, Ltd. p. 957-977,1999.

[2] Paevere, P. and G.C. Foliente, Hysteretic pinching and degradation effects on dynamic response and reliability, in Proceedings of international conference on applications of statistics and probability, 2000. Sydney, Australia.

[3] Medina, R.A. and H. Krawinkler, Influence of hysteretic behavior on the nonlinear response of frame structures. In 13th World Conference on Earthquake Engineering, 2004. Vancouver.

[4] Goda, K., H.P. Hong, and C.S. Lee: Probabilistic characteristics of seismic ductility demand of SDOF systems with Bouc-Wen hysteretic behavior, in Journal of Earthquake Engineering. Taylor & Francis. p. 600-622,2009.

[5] Pu, W. and M. Wu, Ductility demands and residual displacements of pinching hysteretic timber structures subjected to seismic sequences, in Soil Dynamics and Earthquake Engineering. 2018, elsevier sci ltd the boulevard, langford lane, kidlington, oxford ox5 1gb …. p

[6] Gebrekirstos Mezgebo, M. Estimation of Earthquake Input Energy, Hysteretic Energy and its Estimation of Earthquake Input Energy, Hysteretic Energy and its Distribution in MDOF Structures Distribution in MDOF Structures. 2015.

[7] Molazadeh, M. and H. Saffari: The effects of ground motion duration and pinching-degrading behavior on seismic response of SDOF systems, in Soil Dynamics and Earthquake Engineering. Elsevier Ltd. p. 333-347, 2018.

[8] Kazantzi, A.K. and D. Vamvatsikos, The hysteretic energy as a performance measure in analytical studies. Earthquake Spectra, 34(2): p. 719-739, 2018.

[9] McKenna, F., et al., Open System for Earthquake EngineeringSimulation(OpenSees) [Computer Software]. 2000, Pacific Earthquake Engineering Research Center, University of California, Berkeley, CA.

[10] Exponent PU. Saws Model (OpenSees User Documentation). 2010; Available from: http://opensees.berkeley.edu/wiki/index.php/SAWS_Material.

[11] Zhou, L., Structural Response of Mid-rise Hybrid Building System Consisting of a Light Wood Frame Structure and Stiff Core. 2015, University of New Brunswick.

[12] Judd, J.P. and F.S. Fonseca, Analytical model for sheathing-to-framing connections in wood shear walls and diaphragms. Journal of structural engineering. 131(2): p. 345-352, 2005.

[13] Fischer, D., et al., Shake table tests of a two-story house. CUREE publication No. W-06, Richmond, Calif, 2001.

[14] He, M., F. Lam, and R.O. Foschi: Modeling three-dimensional timber light-frame buildings. Journal of structural engineering. 127(8): p. 901-913, 2001.

[15] Pardoen, G.C., Testing and analysis of one-story and two-story shear walls under cyclic loading. 2003: CUREE.

[16] Xu, J., Development of a general dynamic hysteretic light-frame structure model and study on the torsional behavior of open-front light-

frame structures. 2006, Washington State University.
[17] Dinehart, D.W., R.M. Hoffman, and A.S. Blasetti. Finite Element Modeling of Wood Shear Walls with VE Polymers. In 9th World Conference on Timber Engineering, 2006. Portland, Oregon, USA
[18] Pei, S. and J. Van de Lindt: Coupled shear-bending formulation for seismic analysis of stacked wood shear wall systems. Earthquake engineering & structural dynamics. 38(14): p. 1631-1647, 2009.
[19] Sartori, T. and R. Tomasi:, Experimental investigation on sheathing-to-framing connections in wood shear walls. Engineering Structures. 56: p. 2197-2205, 2013.
[20] Germano, F., G. Metelli, and E. Giuriani: Experimental results on the role of sheathing-to-frame and base connections of a European timber framed shear wall. Construction and Building Materials. 80: p. 315-328, 2015.
[21] Verdret, Y., et al.: Experimental investigation on stapled and nailed connections in light timber frame walls. Construction and Building Materials. 91: p. 260-273, 2015.
[22] Mulder, M.J., Numerical modeling of seismic performance of light-frame wood buildings. 2017, University of British Columbia.
[23] Branco, J.M., F.T. Matos, and P.B. Lourenço: Experimental in-plane evaluation of light timber walls panels. Buildings. **7**(3): p. 63, 2017.
[24] Foliente, Greg C. Issues in seismic performance testing and evaluation of timber structural systems. In: CSIRO. Building, Construction and Engineering, editor/s. International Wood Engineering Conference; October 28-31, 1996; New Orleans, USA.
[25] Vamvatsikos, D. and C.A. Cornell: Incremental dynamic analysis. Earthquake engineering & structural dynamics. 31(3): p. 491-514, 2002.
[26] Federal Emergency Management Agency. Quantification of Building Seismic Performance Factors: Washington DC, USA: F. p. Report No. FEMA P-695, 2009.
[27] Yeh, C.-T., B. Hartz, and C. Brown: Damping sources in wood structures. Journal of Sound and Vibration. 19(4): p. 411-419, 1971.
[28] Federal Emergency Management Agency. Recommended seismic design criteria for new steel moment-frame buildings: Washington DC, USA: F. p. Report No.FEMA P-350, 2000.